

# **Sensitivity to interaural correlation in the human ascending auditory system: An fMRI investigation**

T.W. Budd<sup>1</sup>, Deborah A. Hall<sup>1</sup>, Miguel S. Gonçalves<sup>1</sup>, Michael A. Akeroyd<sup>1</sup>, John R.  
Foster<sup>1</sup>, Alan R. Palmer<sup>1</sup>, Kay Head<sup>2</sup>, and A. Quentin Summerfield<sup>1</sup>

<sup>1</sup>MRC Institute of Hearing Research, University Park, Nottingham NG7 2RD, UK.

<sup>2</sup>Magnetic Resonance Centre, School of Physics and Astronomy, University of  
Nottingham, Nottingham NG7 2RD, UK.

Corresponding author:

T.W. Budd

School of Behavioural Sciences

The University of Newcastle

Callaghan. NSW 2308

Australia

Ph: +612 4921 5935

Fx: + 612 4921 6980

email: [bb@ihr.mrc.ac.uk](mailto:bb@ihr.mrc.ac.uk)

Running Title: Auditory fMRI and interaural correlation.

## **ABSTRACT**

A listener's sensitivity to the interaural correlation (IAC) of sound plays an important role in several phenomena in binaural hearing. Although IAC has been examined extensively in neurophysiological studies in animals and in psychophysical studies in humans, little is known about the neural basis of sensitivity to IAC in humans. The present study employed functional magnetic resonance imaging to measure blood oxygen level dependent (BOLD) activity in auditory brainstem and cortical structures in human listeners during presentation of band-pass noise stimuli between which IAC was varied systematically. The stimuli evoked significant bilateral activation in the inferior colliculus, medial geniculate body, and auditory cortex. There was a significant positive relationship between BOLD activity and IAC which was confined to a distinct sub-region of primary auditory cortex located bilaterally at the lateral extent of Heschl's Gyrus. Comparison with published anatomical data indicated that this area may also be cytoarchitecturally distinct. Larger differences in activation were found between levels of IAC near unity than between levels near zero. This response pattern is qualitatively compatible with previous measures of psychophysical and neurophysiological sensitivity to IAC.

## INTRODUCTION

The interaural correlation (IAC) of a sound is one measure of the similarity between the waveforms at the left and right ears. IAC has been defined as “the point-by-point correlation coefficient computed ... after an appropriate delay has been imposed on one of the inputs [at the ears] to maximise the correlation” (Grantham, 1995, p. 302-303). In effect, therefore, IAC is a measure of the randomness of the interaural timing differences (ITDs) of the frequency components that made up a sound.

Human listeners can be remarkably sensitive to differences in IAC. For example, they can detect a difference of less than 2% between a test signal and a reference signal with an IAC of 1.0 (e.g. Culling et al., 2001; Gabriel and Colburn, 1981; Jeffress and Robinson, 1962; Pollack and Trittipoe, 1959). This sensitivity may underpin some of the useful functions of binaural processing. For example, a signal can be detected more easily in a masking noise if the signal has a different spatial location to the masker. Psychophysical studies suggest that the size of some aspects of this effect may be determined by sensitivity to IAC (e.g. Durlach et al., 1986; Bernstein and Trahiotis, 1996; Akeroyd and Summerfield, 2000). Changes in the IAC of a noise result in changes in the perceived “width” of the stimulus when presented through headphones. A noise with an IAC of 1.0 is typically perceived as sound with a compact source located at the centre of the head. If the IAC is reduced, then the image broadens, eventually splitting into two separate images, one at each ear, for an IAC of 0.0 (Blauert and Lindemann, 1986).

Neurophysiological studies in animals have provided substantial evidence of the neural basis for sensitivity to binaural information in a pathway projecting from the medial division of the superior olivary complex (MSO) via the inferior colliculus (IC)

and the medial geniculate body (MGB) to primary auditory cortex (Brugge et al., 1969). The MSO is the primary site of convergence of neural input from the two ears. It is the place where neuronal sensitivity to differences in ITD is first observed (Yin and Chan, 1990). This sensitivity arises in a network of delay lines and coincidence detectors which convert differences in time of arrival at the ears into differences in the profile of neural activity across a spatial array of neurons (Jeffress, 1948; Yin et al., 1987). Coincidence detection is equivalent to a cross-correlation of the inputs from the two ears and it is now widely accepted that the extraction of interaural timing information depends on some form of cross-correlation network (Stern and Trahiotis, 1995).

This network can be simulated by filtering the signals presented to the two ears with matched arrays of band-pass filters (simulating frequency analysis in the cochleae) and computing the cross-correlation function between the outputs of the pairs of filters with corresponding centre frequencies (simulating the processes of delay and coincidence detection). The results of such a simulation are plotted in Figure 1 for six noises with values of IAC ranging from 1.0 (top-left panel) to 0.0 (bottom-right panel). In each plot, the y-axis is the center frequency of the bandpass filter (determining the characteristic frequency of the coincidence detector) and the x-axis is an internal time delay (corresponding to differences in the length of the delay lines that drive the coincidence detector). The amplitude of the plot indicates the probability of a coincidence occurring for a particular combination of characteristic frequency and internal delay. The straight “ridge” in the cross-correlation pattern when the IAC is 1.0 is characteristic for such a stimulus, indicating that in all channels the effective ITD is zero. The sweeping arches at other delays arise at integer multiples of the period of each channel (i.e. integer multiples of the reciprocal of the center frequency). For

present purposes, the most important feature is that the prominence of the various ridges declines as the IAC is reduced, becoming random when the IAC is 0.0. These changes in the simulated patterns may underlie the broadening of the perceived width of the stimuli as the IAC is reduced.

Consistent with the general predictions of cross-correlation models, electrophysiological recordings of ITD-sensitive neurons in the IC of the guinea pig show that the response to band-pass noise is strongly influenced by the IAC of the stimuli (Palmer et al., 1999). Further, there is good evidence that the ITD-sensitivity of low-frequency cells in MSO and IC of the cat also reflects a process of interaural cross correlation (Yin et al., 1987). Compatible evidence has also been obtained in the optic tectum of the barn-owl (the avian homologue of the mammalian IC), where the responsiveness of ITD-sensitive neurones declines as the degree of IAC is decreased from unity (Saberri et al., 1998). Moreover, these cells display greater sensitivity to small decreases in IAC from unity than to small increases in IAC from zero. In this respect, they parallel human psychophysical sensitivity to differences in IAC (Culling et al., 2001).

A limitation to further integration of the psychophysical and neurophysiological evidence of sensitivity to IAC is that the psychophysical evidence has largely been obtained in humans, while the neurophysiological evidence is confined to animal studies. Further, since neurophysiological sensitivity to IAC has primarily been examined in the auditory brainstem, there is little evidence of the cortical sensitivity to IAC. In order to obtain such evidence, the present study used functional magnetic resonance imaging (fMRI) to examine the sensitivity of key structures in the human ascending auditory system to variations in the IAC of band-pass noise.

## MATERIALS AND METHODS

### *Participants*

Seventeen right-handed adults, aged between 19 and 52 years, participated. None had a history of neurological impairment and all had pure-tone hearing thresholds within the normal range ( $<20\text{dB HL}$ ) for octave frequencies between 500 and 4000 Hz, inclusive. All participants were familiarized with the scanning environment and task requirements prior to giving written consent. The study was approved by the Nottingham University Medical School Research Ethics Committee.

### *Stimuli*

The stimuli were 900-ms duration band-pass noise bursts (0-1.5 kHz) with 40-ms raised-cosine ramps applied to the onset and offset. Each noise had one of six fixed values ( $\rho$ ) of IAC: 1.00, 0.93, 0.80, 0.60, 0.33 or 0.00. These six levels were determined through piloting testing with experienced listeners (TWB and AQS) and defined approximately equal perceptual steps between noises with IACs of unity and zero (Culling et al., 2001; Pollack and Trittipoe, 1959).

The bandwidth and intensity of the noise stimuli were the same at each ear within conditions and were constant across conditions. The only difference between conditions was the statistical correlation ( $\rho$ ) between the noise signal at each ear. Such stimuli achieve the necessary control over the potentially confounding variables of level and bandwidth when seeking to locate activation that is solely due to a binaural analysis.

The stimuli were generated using Licklider and Dzendolet's (1948) three-noise method (see also Jeffress and Robinson, 1962) implemented in MATLAB (Akeroyd, 2001). The left channel of each stimulus was made by adding one random noise to a second statistically independent noise in a power ratio of  $(\rho):(1-\rho)$ . The right channel

was made by adding the first noise to a third independent noise in the same power ratio. Each initial noise was constructed in the frequency domain, using a 39690-point spectrum buffer with a sampling rate of 44100 Hz. The real and imaginary values of all the frequency points below 1500 Hz were drawn randomly from a Gaussian distribution, whereas the real and imaginary values of all higher-frequency points were set to zero. An inverse Fast Fourier Transform was applied to the resulting spectrum to yield a waveform of 900-ms duration. Raised-cosine ramps of 40-ms duration were then applied to the onset and offset.

Using this procedure, 40 noises with each level of IAC were synthesised. Thirty trains of eight noise bursts were constructed for each level of IAC by randomly selecting subsets of eight exemplars from the set of 40, with replacement, and concatenating them separated by 100-ms silent intervals. With 6 levels of IAC and 30 stimulus trains at each level, 180 stimulus trains were constructed in total (Note 1).

Stimulus trains were presented in a different random order to each participant. Stimuli were presented binaurally through headphones at 72 dB SPL. The headphones were designed for use during fMRI and consisted of electrostatic drivers mounted in industrial ear defenders (Palmer et al., 1998).

### *fMRI Acquisition*

Images were acquired using a 3T whole-body MRI system equipped with a head gradient coil and a birdcage radio-frequency receiver coil (Bowtell et al., 1994). Contiguous multi-slice T2-weighted images were acquired using echo-planar imaging (EPI) (TE < 40 ms; flip angle 90 degrees). Each whole-head volume was acquired in the coronal orientation (44 slices; 4 mm<sup>3</sup> voxels; 64 x 64 matrix; 3.4 s/volume) every 11.6 s. A stimulus train was delivered during the 8.2-s interval between volume acquisitions. This clustered and ‘sparse’ imaging technique reduces the influence of

scanner noise on the blood oxygen level dependent (BOLD) response to the auditory stimulus of interest (Edmister et al., 1999; Hall et al., 1999). In addition to the 180 volumes which were acquired on trials when a stimulus train was presented, 30 volumes, preceded by an 8.2-s silent interval were acquired at random intervals to provide an estimate of baseline BOLD activity. For each subject, 107 volumes were acquired in each of two sequential scanning sessions, giving a total of 214 volumes.

### *Task*

During imaging, participants lay supine in the MR scanner with their eyes closed. They were instructed to make a button press with their right index finger immediately after each volume acquisition. Responses were scored as correct if they were made within 2 s of the end of the volume acquisition.

### *Data Analysis*

EPI data were analysed with the SPM99 software package (<http://www.fil.ion.ucl.ac.uk/spm/spm99>). The first two volumes in each session were excluded to avoid T1 relaxation effects. The remaining 210 volumes were submitted to the analysis sequence described below.

### *Image pre-processing*

Motion-corrected images were computed for each participant's EPI time series. Movement did not exceed a translation of 3 mm or a rotation of 3° (with the majority of translations and rotations being less than 1 mm or 1°). An AVI-format animation was created from each motion-corrected image time-series and visually examined. No residual movement could be detected in any time-series. A motion-corrected mean image was also computed for each participant and was coregistered and spatially normalised to a standardised brain space using a modified version of the SPM EPI template which incorporated the signal loss in the middle and inferior temporal lobes

observed at 3T. The brain space was defined by the Montreal Neurological Institute (MNI). The resulting transformation parameters were then applied to all images, creating a set of images with a 2-mm<sup>3</sup> voxel resolution. These realigned and spatially normalised images were then smoothed, using an 8-mm Full-Width Half-Maximum Gaussian filter, high-pass filtered (<160 s), scaled to the global mean intensity and corrected for first-order auto-correlation.

#### *Anatomical localisation of functional activity*

Three *a priori* regions of interest (ROIs) were defined via visual inspection of a high-resolution (1 mm<sup>3</sup>) single-subject normalised structural image provided by the MNI (“COLIN27” see Brett et al., 2002), which occupied the same MNI space as the normalised EPI images. Using previously established procedures (Griffiths et al., 2001; Harms and Melcher, 2002; Rademacher et al., 2002), IC, MGB, and superior temporal gyrus (STG) were identified in the COLIN27 image. ROIs corresponding to left and right IC and MGB were defined by placing a sphere of 5-mm radius at the anatomically-defined centre of each nucleus: (XYZ mm: IC left: -4 -34 -12; IC right: +6 -35 -12; MGB left: -15 -26 -7; MGB right: +16 -25 -7).

A third ROI that encompassed the auditory cortex (AC) on the STG, extending into the lateral and superior temporal sulci, was created to provide an *a priori* volume for correction for multiple comparisons across voxels in the auditory cortex. This ROI incorporated primary and non-primary subdivisions of auditory cortical regions (Galaburda and Sanides, 1980; Morosan et al., 2001; Penhune et al., 1996; Rademacher et al., 2001; Rivier and Clarke, 1997; Westbury et al., 1999). Since these subdivisions probably correspond to functional differences in perceptual processing, a more comprehensive definition of the anatomical location of BOLD activity within AC was carried out as follows.

Initially, spatial coordinates of activation maxima were transformed from MNI space into Talairach space (Brett et al., 2002) in order to use an automated labelling system for grey/white matter and for Brodmann areas (Lancaster et al., 2000). While the anatomical localisation of fMRI activity using the Brodmann and Talairach reference systems provides only general information regarding auditory cortical anatomy, it establishes a basis for comparison with regions of activation reported in previous auditory fMRI studies.

Anatomically-defined probability maps of auditory cortical regions that already occupied the MNI spatial reference system (Johnsrude, 2001) were also used to define the location of regions of activation. These include probability maps of the morphological borders of Heschl's gyrus (HG) (Penhune et al., 1996) and planum temporale (PT) (Westbury et al., 1999). Probability maps of 3 putative subdivisions of the primary auditory cortex, based on cytoarchitectural criteria, have also been defined (Morosan et al., 2001; Rademacher et al., 2001). These subdivisions are termed Te1.1, Te1.0, and Te1.2, and are placed along the medial-lateral axis of HG. Since the original probability values for each map reflect a different scale, all values were rescaled to the maximum probability value within each map in order to allow meaningful between-map comparisons to be made.

The combination of probabilistic maps with the Talairach and Brodmann reference systems provides converging evidence for, and a means to distinguish between, neurophysiologically and morphologically distinct regions of the auditory cortex.

### *Statistical Parametric Mapping*

The EPI image time series were analysed using an epoch-based general linear model analysis (Friston et al., 1995). The relationship between BOLD activity and

IAC level was examined using the successive forward modelling of orthogonal polynomial terms (Buchel et al., 1998). In this approach, t-statistic images were generated to reveal those voxels where BOLD activity showed a significant relationship with IAC level in terms either of 0<sup>th</sup>-order (all IAC levels vs silence), 1<sup>st</sup>-order (linear), or 2<sup>nd</sup>-order (quadratic) covariation. The 0<sup>th</sup>-order term is equivalent to a simple statistical subtraction of the silent baseline from conditions involving noise stimulation (i.e box-car). Therefore voxels showing a significant 0<sup>th</sup>-order effect of IAC revealed those brain regions where a significant increase in activity occurred in response to noise stimulation relative to the silent baseline. Voxels showing a significant 1<sup>st</sup>-order effect show indicated regions where activity changed linearly with IAC level after any variance associated with the 0<sup>th</sup>-order term had been taken into account. Similarly, voxels showing a significant 2<sup>nd</sup>-order effect indicated regions where activity changed quadratically with IAC level after accounting for the 0<sup>th</sup>- and 1<sup>st</sup>-order variations. These parametric analyses of the relationship between BOLD and IAC were initially applied to the data of individual subjects so that a subsequent random-effects group analysis could be undertaken (Friston et al., 1999).

The two acquisition sessions were modelled as a single session. Two covariates specifying each session were included in the analysis model for each individual subject to control for any residual session effect. Six realignment parameters (yaw, pitch, and roll rotations and x, y, and z translations), obtained from the motion correction procedure, were also included as covariates of no interest. Covariates based on orthogonal polynomial expansions of IAC level (assuming equal intervals between adjacent IAC levels) were successively added to the model, until the addition of the next term did not significantly improve the model fit. Group SPM t-statistic images

were then computed for each order of the polynomial basis functions using the SPM random-effects approach.

Significance thresholds for IC and MGB were calculated according to the spatial extent method of Friston (1997) using all suprathreshold voxels ( $p < 0.001$ , uncorrected) within the regions defining IC or MGB, respectively. Significance thresholds in the region defined by AC were adjusted for multiple comparisons ( $p < 0.05$ , corrected) using a small-volume correction based on the total number of voxels within the region defined by AC.

## RESULTS

### *Task Performance*

Table 1 lists the percentages of volume acquisitions for which participants made a button press within the permitted 2-s window. The across-condition average of 86% did not vary with IAC level (one-way ANOVA,  $p > 0.05$ ). This result indicates that participants maintained an adequate, and uniform, level of arousal across conditions.

<<TABLE 1>>

### *Inferior Colliculus and Medial Geniculate Body*

Figure 2 shows group t-statistic images of all suprathreshold voxels for the 0<sup>th</sup>-order polynomial effect of IAC ( $p < 0.001$ , uncorrected) for brain-stem and subcortical regions. Figure 2a illustrates the close correspondence between these regions of activation and the anatomical location of IC. The spatial extent of activation for left and right IC was 43 and 40 voxels, respectively. The probability of obtaining activation with this spatial extent was significantly greater than chance ( $p < 0.05$ ) for the SPM component smoothness in the EPI images (9.65 voxels) (see Friston, 1997). The peaks of activation were located at  $x = -4$ ,  $y = -38$ ,  $z = -10$  mm and  $x = +4$ ,  $y = -34$ ,  $z = -12$

mm. These locations are within 4.5 mm and 2.2 mm of the anatomically-defined centres of the left and right inferior colliculi, respectively. At these peak locations, the noise conditions generated a 4.9% (left) and a 3.7% (right) increase in the response relative to the silent baseline. For the 0<sup>th</sup>-order effect in MGB, only one and two voxels survived threshold ( $p < 0.001$ , uncorrected) on the left and right, respectively (Note 2) (Figure 2b). This activation failed to reach the spatial extent threshold of 9.65 voxels. No suprathreshold voxels for either the linear or quadratic polynomial term were found in either IC or MGB and no other brain-stem or subcortical regions showed any significant activation.

<<FIGURE 2>>

The foregoing results indicate that significant activation to the noise stimuli relative to the silent baseline was obtained in IC, but that this activation did not vary with IAC level. In MGB, there was no significant activation for the noise stimuli, nor was there any variation in activity with IAC level (Note 3).

#### *Auditory Cortex 0<sup>th</sup>-order Effects*

Figure 3a shows the t-statistic image for all suprathreshold voxels for the 0<sup>th</sup>-order polynomial term ( $p < 0.05$ , corrected). These voxels were almost entirely confined to auditory cortical regions. Comparison of Figures 3a and 3b demonstrates the close correspondence between the location of activation and the regions covered by the probability maps for HG, PT, and primary auditory cortex.

<<FIGURE 3>>

Table 2 lists standardised coordinates, anatomical locations, and probability-map results for four distinct maxima of activation found for the 0<sup>th</sup>-order polynomial term (Figure 3a). All maxima were located within primary and adjacent non-primary auditory regions of the STG. The most medial maxima in the left and right

hemispheres showed the highest probabilities of lying within HG according to Penhune's map. These maxima also show the highest probabilities of falling within 'core-like' (Te1.0) and 'non-core-like' (Te1.1) regions of primary auditory cortex according to Morosan's maps.

<<TABLE 2>>

Only the most medial maximum in left hemisphere was labelled as primary auditory cortex (BA 41) according to the automated labelling system (Lancaster et al., 2000). The most medial maximum in right hemisphere was labelled as BA22, suggesting a location anterior to primary auditory cortex, although the corresponding Talairach label was HG. While the Brodmann and Talairach labels, at best, provide only a general guide to the anatomical locations of activation, the medial maxima in both hemispheres are located within spatially extended clusters of activation which follow the typical oblique orientation of HG, and which largely incorporate the medial aspects of HG. The medial activation overlaps with the medial two-thirds of HG and Te1.0, indicating that activation encompasses primary auditory cortex.

In contrast to the relatively symmetric location and orientation of the more medial maxima, the more lateral maxima were asymmetric, being located in BA22 and BA42. The most lateral maximum in the right hemisphere occupied the most anterior location of any of the four maxima, with a relatively low probability for Penhune's map of HG but with higher probabilities for Morosan's Te1.0 and Te1.2 regions (Figure 3b). The right lateral peak suggests a location in either the core or non-core like regions of primary auditory cortex (Morosan et al., 2001). In contrast the most lateral maximum in the left hemisphere was the most posterior of the four maxima and showed the highest overall probability for the non-primary auditory region, PT, according to

Westbury's probability map, with no corresponding values for either Morosan's or Penhune's maps.

#### *Auditory Cortex 1<sup>st</sup>-order Effects*

A significant linear effect (1<sup>st</sup>-order polynomial) was found in two bilateral regions anterolaterally in HG (Figure 4a). The introduction of the linear polynomial term led to a significant ( $p < 0.05$ , corrected) improvement in fit between BOLD activity and IAC level, beyond that already accounted for by the 0<sup>th</sup>-order term. This result reveals that BOLD activity in these discrete and anatomically symmetric cortical regions showed a significant and positive linear relationship with IAC level. No additional suprathreshold voxels were found by adding a 2<sup>nd</sup>-order polynomial term to the analysis model. Similarly, no suprathreshold voxels were found for the negative 1<sup>st</sup>-, or 2<sup>nd</sup>-order polynomial terms. The more widespread regions of bilateral activation found for the 0<sup>th</sup>-order polynomial term are absent from Figure 4a. This result indicates that most of the activity in STG in the 0<sup>th</sup>-order t-statistic images (Figure 3a) reflected a general activation to a noise stimulus, rather than any specific sensitivity to IAC level.

<<FIGURE 4>>

<<TABLE 3>>

Table 3 lists the standardised coordinates, anatomical labels, and probability-map values for the peak voxels in the two symmetric bilateral regions in Figure 4a where activity showed a significant linear effect of IAC. At these two locations, the noise conditions generated a 4.9% and a 4.1% increase in the response in the left and right hemispheres, respectively, relative to the silent baseline. In comparison, the difference between the response for IAC levels of zero and unity ranged from 0.4% and 0.3%.

Thus, the effect of IAC represents a small proportion of the overall BOLD sensitivity to stimulation by noise.

Figure 4b illustrates the results of the probability-map analysis for the linear effect of IAC. This analysis reveals that all 18 suprathreshold voxels (14 left; 4 right) which showed a significant linear covariation with IAC level were located within a non-core region of primary auditory cortex (Te1.2). This pattern can be distinguished from the activated regions for the 0<sup>th</sup>-order analysis (Figure 3a) as the probability map values for HG and PT are lower, and the values for Te1.2 are higher, for both the left- and right-hemisphere activation maxima. Therefore, the cortical regions which showed a consistent covariation with IAC were confined to the antero-lateral extent of primary auditory cortex. These were anatomically distinct from the cortical regions where the greatest increases in BOLD activity relative to the silent baseline were observed (i.e Te1.0).

<<FIGURE 5>>

Figure 5 shows, for each IAC level, the mean raw (adjusted) BOLD activity averaged over all 18 suprathreshold voxels where a significant and positive linear effect of IAC level was obtained. The moderate departure from linearity of BOLD signal magnitude follows a positive accelerating function of IAC level. The smallest increase occurred between IAC levels 0.00 and 0.33, and the largest increase occurred between IAC levels 0.93 and 1.00.

## DISCUSSION

### *IAC sensitivity in auditory cortex*

Auditory cortical regions showed the greatest sensitivity to IAC of the three anatomical areas examined. The analysis provided evidence of a discrete bilateral cortical region where BOLD activity showed a significant linear increase with increasing IAC level. This linear covariation between BOLD activity and IAC level was confined to two bilateral and symmetric regions in the lateral part of HG. These regions correspond to a cytoarchitecturally-distinct subdivision of primary auditory cortex, Te1.2, as defined in anatomical studies (Morosan et al., 2001). The anatomical location of these IAC-sensitive regions can be distinguished from other auditory cortical regions where suprathreshold values were found in the 0<sup>th</sup>-order polynomial effect (Figure 3a). These other regions responded to noise, irrespective of the level of IAC, and were located posteriorly along the medial two-thirds of HG (Penhune et al., 1996) in primary auditory cortex (Te1.0 and Te1.1) (Morosan et al., 2001) as well as PT (Westbury et al., 1999).

Region Te1.2 has been described as a ‘transitional zone’ between primary and non-primary auditory fields (Morosan et al., 2001). While Te1.2 shares the typical features of a primary sensory area (i.e. small granular cells, prominent layer IV), it can be distinguished from core regions of primary auditory cortex as a result of a broader layer III which contains clusters of medium size IIIc pyramid cells (Morosan et al., 2001). These same features are also found in surrounding ‘belt’ regions of auditory cortex (Hackett et al., 2001). The present results suggest that the anatomically-distinct auditory cortical region, Te1.2, may also represent a functionally distinct auditory cortical region in terms of sensitivity to IAC.

The observed anatomical specificity of IAC sensitivity may reflect a cortical specialisation for binaural analysis in low frequency regions of auditory cortex. Non-human primate research has shown that cells in macaque primary auditory cortex with low characteristic frequencies are more likely to show ITD sensitivity (Brugge et al., 1969) and binaural interactions (Reser et al., 2000) than are high-frequency cells. In humans, recent fMRI studies indicate that anterior-lateral regions of HG show the greatest specificity to low frequency sounds (<660 Hz) (Schonwiesner et al., 2002; Talavage et al., 2000). The reported Talairach coordinates of the centres of low-frequency responsive cortical fields (Talavage et al.: 53.6, -1.3, 1.7 and -51.9, -16.3, 9.0; Schonwiesner et al.: -47.4, -11.1, 7.0-mm) are close to the Talairach coordinates of IAC sensitivity maxima found within region Te1.2 in the present study (-55, -8, 2-mm). The possibility that IAC-sensitive regions of human auditory cortex are located in regions which respond preferentially to low frequency stimulation is entirely consistent with neurophysiological and psychophysical evidence that sensitivity to ITD and IAC is largely confined to low frequency stimulation (Yin et al., 1987).

An alternative to the interpretation that region Te1.2 plays a specific role in the analysis or representation of binaural information, is that the sensitivity of Te1.2 to IAC may reflect a more general role in the analysis of sounds in which temporal patterning is displayed across frequency. Support for the latter role comes from the demonstration that the region is activated not only by IAC but also by another type of acoustic signal that requires time-interval processing and across-frequency integration. “Iterated rippled noise” (IRN) has a pitch whose strength is determined by the temporal regularity of the signal (e.g. Yost et al., 1996). Griffiths et al. (1998), in a neuro-imaging study, demonstrated that activation in the lateral part of HG increased systematically with the degree of temporal regularity of an IRN. Unlike IAC, the

temporal regularity in an IRN is determined by the monaural input from each ear, rather than by a binaural comparison of the input from the two ears. However, just as the salience of IAC is conveyed by the relationship between the cross-correlation pattern in many frequency channels (Figure 1), so the salience of the pitch in an IRN is greatest when the period of the temporal patterning is consistent across frequency channels (Figure 1 in Griffiths et al., 1998). In the case of IAC, the integration across frequency occurs after the initial computation of cross-correlation and is apparent at the level of the IC (Mori, 1997). However, precisely how binaural temporal information is combined across frequency channels and refined at higher auditory centres remains unresolved (Saber et al., 1998; Shackleton et al., 1992; Stern and Trahiotis, 1995). Nonetheless, the regions shown to be sensitive to binaural temporal regularity in the present study are close to the regions shown to be sensitive to monaural temporal regularity in the study of Griffiths et al. (1998). This correspondence suggests that region Te1.2 could also be specialised for the across-frequency integration of evidence of detailed temporal patterning.

*IAC sensitivity in inferior colliculus and medial geniculate body.*

No significant relationship was found between IAC and BOLD activity in IC or MGB. This result was unexpected given evidence from electrophysiological recordings in animals that cells in IC are sensitive to the degree of interaural correlation in band-pass noise stimuli (Palmer et al., 1999; Saber et al., 1998). BOLD activity in IC has also proved to be a sensitive measure of variations in some characteristics of monaural acoustic stimulation. This result has been demonstrated for variations in temporal characteristics of both the fine structure and the envelope of sounds (Giraud et al., 2000; Griffiths et al., 1998; Ackermann et al., 2001; Harms et al., 2002).

Several explanations might account for the lack of BOLD sensitivity to IAC level in IC. One possibility is that cardiac gating of EPI volume acquisition was not used in the present experiment. This technique has been employed previously to reduce the effects on EPI images of the pulsatile motion of brainstem structures that accompanies the cardiac cycle (Guimaraes et al., 1998). The absence of cardiac gating may have reduced the sensitivity of fMRI to small differences in BOLD activity in IC. This possibility seems unlikely, however, given that the effect size of the activation to noise relative to the silent baseline in IC was as large as that found in auditory cortical regions. Also, BOLD sensitivity in IC to variations in stimulus rate without cardiac gating has been reported in previous auditory fMRI studies (Ackermann et al., 2001).

Another possibility is that the changes in neural activity reported in single-unit studies in animals following manipulation of IAC are not manifest as increases or decreases in the overall level of neural activity as reflected in the BOLD response. In fact, complex interactions of excitatory and inhibitory potentials occur in IC (Oliver, 2000). These interactions subserve the integration of across-frequency ITD information between neurons in the external and central nuclei of the IC and are thought to resolve phase ambiguities in individual spectral channels carrying ITD information (Mori, 1997). These complex interactions may not be manifest as changes in the regional haemodynamic activity that is reflected in the BOLD response.

#### *The psychophysical basis of IAC sensitivity in auditory cortex*

The positively accelerating form of the relationship between BOLD activity and IAC level found in region Te1.2 is identical to the form consistently reported in psychophysical studies in humans as well as in intracellular recordings from the auditory brain stem of animals. In the present study, smaller increases in BOLD signal were found when IAC was increased from 0 to 0.33 and from 0.33 to 0.60 than when

IAC was increased from 0.93 to 1.00 (Figure 5). Compatibly, human listeners are more sensitive to differences in IAC close to unity than zero (Culling et al., 2001; Gabriel and Colburn, 1981; Pollack and Trittipoe, 1959). Therefore, the same size of change in interaural correlation leads to a larger perceptual change at an IAC near 1.0 than at an IAC near 0.0.

The correspondence of the relationship between BOLD activity and IAC, on the one hand, and perceptual sensitivity to differences in IAC, on the other hand, suggests that the IAC-dependent cortical activity may reflect perceptual processes involved in listener's sensitivity to IAC. Whatever the perceptual role of the neural process reflected in the sensitivity of lateral auditory cortical regions to IAC, it is almost certain that this process involves an abstract representation of binaural temporal information. IAC-sensitive cortical activity could not reflect the analysis of the fine temporal structure of binaural information itself, because this detail is translated from a time-code to a place code at an earlier stage in the ascending auditory system. That transformation starts in the medial superior olive and is essentially complete at the level of the IC (Eggermont, 2001; Palmer, 1995). Therefore the primary calculation of the level of IAC in a stimulus could not be performed in the auditory cortical regions that displayed parametric sensitivity to IAC. It seems more likely that the activity in these regions reflects higher-order analyses, possibly those that underpin a listener's sensitivity to variations in the compactness of the stimuli according to their value of IAC.

In summary, the present results provide evidence for a cytoarchitecturally-distinct region of the auditory cortex that is sensitive to subtle variations in binaural characteristics of sound. The sensitivity observed to the degree of interaural correlation of low-frequency band-pass noise is compatible with the perceptual

sensitivity of human listeners to interaural correlation established in psychophysical studies. The finding that the lateral part of HG in human auditory cortex is sensitive to subtle changes in the binaural characteristics of acoustic stimuli provides a basis for future examinations of binaural hearing using fMRI.

## **ACKNOWLEDGEMENTS**

This study was supported in part by MRC project grant G9302591 to the Magnetic Resonance Centre, University of Nottingham. The authors thank Ingrid Johnsrude, Virginia Penhune, Robert Zatorre, Chris Westbury, Marc Bouffard, Jorg Rademacher, Karl Zilles, and Katrina Amunts for advice and assistance in providing the probability maps of auditory cortex. The authors also thank two anonymous reviewers for criticisms that lead to improvements in the manuscript.

## NOTES

Note 1: Due to a programming error, in some conditions some subjects received either 29 or 31 stimulus trains. As a result, the mean number of trains across subjects for each of the 6 levels of IAC was 29.8, 30.2, 30.1, 29.6, 29.8, and 29.8.

Note 2: Relatively large suprathreshold clusters were obtained bilaterally in MGB in a fixed-effects group analysis. This difference from the results of the random-effects analysis was due to the contribution of one experimental condition only ( $\rho=1.0$ ), reinforcing the view that the results of fixed-effects group analyses may not be generalisable (see also Note 3).

Note 3: In a separate analysis, t-statistic maps were generated for each IAC level relative to the silent baseline. These maps displayed a significantly larger extent of activation when the IAC level was 1.0, relative to the remaining IAC levels, in both auditory cortical regions and MGB, but not IC. Unlike the reported parametric analyses, the extent of activation when the IAC level was 1.0 survived statistical thresholding in MGB.

## REFERENCES

- Ackermann, H, Riecker, A, Mathiak, K, Erb, M, Grodd, W and Wildgruber, D (2001). "Rate-dependent activation of a prefrontal-insular-cerebellar network during passive listening to trains of click stimuli: an fMRI study." *Neuroreport* 12(18): 4087-92.
- Akeroyd, M A 2001 A Binaural Cross-correlogram Toolbox for MATLAB [http://www.biols.susx.ac.uk/Home/Michael\\_Akeroyd/](http://www.biols.susx.ac.uk/Home/Michael_Akeroyd/)
- Akeroyd, M A and Summerfield A Q. (2000). Integration of monaural and binaural evidence of vowel formants. *Journal of the Acoustic Society of America*; 107: 3394-406.
- Bernstein, L R and Trahiotis, C. (1996). The normalized correlation: accounting for binaural detection across center frequency. *Journal of the Acoustic Society of America* 100(6): 3774-84.
- Blauert, J and Lindemann, W (1986). "Spatial mapping of intracranial auditory events for various degrees of interaural coherence." *Journal of the Acoustic Society of America* 79(3): 806-813.
- Bowtell, R, Mansfield, P, Coxon, R J, Harvey, R J and Glover, P M (1994). "High-resolution EPI at 3.0 T." *Magn Reson Mater Phys Med Biol* 2: 1-5.
- Brett, M, Johnsrude, I S and Owen, A M (2002). "The problem of functional localisation in the human brain." *Nature Reviews neuroscience* 3: 243-250.
- Brugge, J F, Dubrovsky, N A, Aitkin, L M and Anderson, D J (1969). "Sensitivity of single neurons in auditory cortex of cat to binaural tonal stimulation: effects of varying interaural time and intensity." *Journal of Neurophysiology* 32: 1005-1024.

- Buchel, C, Holmes, A P, Rees, G and Friston, K J (1998). "Characterizing stimulus-response functions using nonlinear regressors in parametric fMRI experiments." *NeuroImage* 8(2): 140-148.
- Culling, J F, Colburn, H S and Spurchise, M (2001). "Interaural correlation sensitivity." *Journal of the Acoustic Society of America* 110(2): 1020-1029.
- Durlach NI, Gabriel KJ, Colburn HS, Trahiotis C (1986). Interaural correlation discrimination: II. Relation to binaural unmasking. *Journal of the Acoustical Society of America* 79(5): 1548-57.
- Edmister, W B, Talavage, T M, Ledden, P J and Weisskoff, R M (1999). "Improved auditory cortex imaging using clustered volume acquisitions." *Human Brain Mapping* 7(2): 89-97.
- Eggermont, J J (2001). "Between sound and perception: reviewing the search for a neural code." *Hear Res* 157(1-2): 1-42.
- Friston, K J (1997). "Testing for anatomically specified regional effects." *Human Brain Mapping* 5: 133-136.
- Friston, K J, Holmes, A P, Price, C J, Buchel, C and Worsley, K J (1999). "Multisubject fMRI studies and conjunction analysis." *NeuroImage* 10: 385-396.
- Friston, K J, Holmes, A P, Worsley, K J, Poline, J P, Frith, C D and Frackowiak, R S J (1995). "Statistical Parametric Maps in Functional Imaging: A General Linear Approach." *Human Brain Mapping* 2: 189-210.
- Gabriel, K J and Colburn, H S (1981). "Interaural correlation discrimination. I Bandwidth and level dependence." *The Journal of the Acoustical Society of America* 69: 1394-1401.
- Galaburda, A and Sanides, F (1980). "Cytoarchitectonic organisation of the human auditory cortex." *Journal of Comparative Neurology* 190: 597-610.

- Giraud, A L, Lorenzi, C, Ashburner, J, Wable, J, Johnsrude, I, Frackowiak, R and Kleinschmidt, A (2000). "Representation of the temporal envelope of sounds in the human brain." *J Neurophysiol* 84(3): 1588-98.
- Grantham, D W (1995). *Spatial Hearing and Related Phenomena*. Hearing. B. C. J. Moore. London, Academic Press: 297-345.
- Griffiths, T D, Buchel, C, Frackowiak, R S and Patterson, R D (1998). "Analysis of temporal structure in sound by the human brain." *Nat Neurosci* 1(5): 422-7.
- Griffiths, T D, Uppenkamp, S, Johnsrude, I S, Josephs, O and Patterson, R D (2001). "Encoding of the temporal regularity of sound in the human brainstem." *Nature Neuroscience* 4(6): 633-637.
- Guimaraes, A R, Melcher, J R, Talavage, T M, Baker, J R, Ledden, P, Rosen, B R, Kiang, N Y, Fullerton, B C and Weisskoff, R M (1998). "Imaging subcortical auditory activity in humans." *Hum Brain Mapp* 6(1): 33-41.
- Hall, D A, Haggard, M P, Akeroyd, M A, Palmer, A R, Summerfield, A Q, Elliott, M R, Gurney, E M and Bowtell, R W (1999). "'Sparse' temporal sampling in auditory fMRI." *Human Brain Mapping* 7(3): 213-223.
- Harms, M P and Melcher, J R (2002). "Sound repetition rate in the human auditory pathway: representations in the waveshape and amplitude of fMRI activation." *Journal of Neurophysiology* 88: 1433-1450.
- Jeffress, L A (1948). "A place theory of sound localization." *J. Comp. Physiol. Psychol* 61: 468-486.
- Jeffress, L A and Robinson, D E (1962). "Formulas for the coefficient of correlation for noise." *Journal of the Acoustic Society of America* 34: 1658-1659.
- Johnsrude, I (2001). "Cytoarchitectonic region-of-interest analysis of auditory imaging data." *NeuroImage* 13: S891.

- Lancaster, J L, Woldorff, M G, Parsons, L M, Liotti, M, Freitas, C S, Rainey, L, Kochunov, P V, Nickerson, D, Mikiten, S A and Fox, P T (2000). "Automated Talairach atlas labels for functional brain mapping." *Hum Brain Mapp* 10(3): 120-31.
- Licklider, J C R and Dzendolt, E (1948). "Oscillographic scatterplots illustrating various degrees of correlation." *Science* 107: 121-124.
- Mori, K (1997). "Across-frequency nonlinear inhibition by GABA in processing of interaural time differences." *Hearing Research* 111: 22-30.
- Morosan, P, Rademacher, J, Schleicher, A, Amunts, K, Schormann, T and Zilles, K (2001). "Human primary auditory cortex: Cytoarchitectonic subdivisions and mapping into a spatial reference system." *NeuroImage* 13(4): 684-701.
- Oliver, D L (2000). "Ascending efferent projections of the superior olivary complex." *Microsc Res Tech* 51(4): 355-63.
- Palmer, A R (1995). *Neural Signal Processing. Hearing*. B. C. J. Moore. London, Academic Press: 75-121.
- Palmer, A R, Bullock, D C and Chambers, J D (1998). "A high-output, high-quality sound system for use in auditory fMRI." *NeuroImage* 7: S359.
- Palmer, A R, Jiang, D and McAlpine, D (1999). "Desynchronizing Responses to Correlated Noise: A Mechanism for Binaural Masking Level Differences at the inferior Colliculus." *Journal of Physiology*: 722-734.
- Patterson RD, Allerhand MH, Giguere C (1995). Time-domain modeling of peripheral auditory processing: a modular architecture and a software platform. *Journal of the Acoustical Society of America* 98(4):1890-4.
- Penhune, V B, Zatorre, R J, MacDonald, J D and Evans, A C (1996). "Interhemispheric anatomical differences in human primary auditory cortex: probabilistic mapping

- and volume measurement from magnetic resonance scans." *Cereb Cortex* 6(5): 661-72.
- Pollack, I and Trittipoe, W J (1959). "Binaural Listening and Interaural Noise Correlation." *The Journal of the Acoustical Society of America* 31(9): 1250-1252.
- Rademacher, J, Burgel, U and Zilles, K (2002). "Stereotaxic Localization, Intersubject Variability, and Interhemispheric Differences of the Human Auditory Thalamocortical System." *NeuroImage* 17: 142-160.
- Rademacher, J, Morosan, P, Schormann, T, Schleicher, A, Werner, C, Freund, H-J and Zilles, K (2001). "Probabilistic mapping and volume measurements of human primary auditory cortex." *NeuroImage* 13: 669-683.
- Rivier, F and Clarke, S (1997). "Cytochrome oxidase, acetylcholinesterase, and NADPH-diaphorase staining in human supratemporal and insular cortex: evidence for multiple auditory areas." *NeuroImage* 6(4): 288-304.
- Saberi, K, Takahashi, Y, Konishi, M, Albeck, Y, Arthur, B J and Farahbod, H (1998). "Effects of interaural decorrelation on neural and behavioral detection of spatial cues." *Neuron* 21(4): 789-98.
- Shackleton, T M, Meddis, R and Hewwit, M J (1992). "Across frequency integration in a model of lateralization." *Journal of the Acoustic Society of America* 91: 2276-2279.
- Stern, R M and Trahiotis, C (1995). *Models of Binaural Interaction. Hearing*. B. C. J. Moore. London, Academic Press Limited: 347-386.
- Westbury, C F, Zatorre, R J and Evans, A C (1999). "Quantifying variability in the planum temporale: A probability map." *Cerebral Cortex* 9(4): 392-405.
- Yin, T C T and Chan, J C K (1990). "Interaural time sensitivity in medial superior olive of cat." *Journal of Neurophysiology* 64(465-488).

Yin, T C T, Chan, J C K and Carney, L (1987). "Effects of interaural time delays of noise stimuli on low frequency cells in the cat's inferior colliculus. III. Evidence for cross-correlation." *Journal of Neurophysiology* 58: 562-583.

Yost WA, Patterson R, Sheft S. (1996). A time domain description for the pitch strength of iterated rippled noise. *Journal of the Acoustical Society of America* 99(2): 1066-78.

## FIGURE CAPTIONS

**Figure 1:** Binaural cross-correlograms of band-pass noises (0-1500Hz) with six levels of IAC ranging from zero to unity. The waveforms that would be presented to each ear were analysed with two banks of 40 gammatone filters with centre frequencies ranging from 100 to 1500 Hz equally spaced on an ERB scale (Patterson, Allerhand, and Giguere, 1995). Each line in the correlogram is the cross-correlation function computed between the outputs of pairs of filters with corresponding centre frequencies (vertical axis). Each point on each line is the sum of cross-products of the amplitudes of samples in the two waveforms after a delay in the range from  $-2000 \mu\text{s}$  to  $+2000 \mu\text{s}$  was imposed on one of the waveforms (horizontal axis).

**Figure 2:** (a) Group random-effects SPM t-statistic images for the 0<sup>th</sup>-order polynomial term for three orthogonal slices centred on the anatomically defined IC (white circles) superimposed on an individual T1 image; (b) Images as in (a) but with slices centred on the anatomical centre of MGB. All maps show t values for uncorrected threshold; where  $t > 3.69$  ( $p < 0.001$ ). Slice positions ( $\pm$  white) are given in MNI xyz mm coordinates.

**Figure 3:** (a) Group random-effects t-statistic images for the 0<sup>th</sup>-order polynomial term, superimposed over an individual T1 image. Slice positions ( $\pm$  white) are given in MNI z coordinates for 4 axial slices centred on STG. (AC small-volume corrected thresholds,  $t > 5.22$ ,  $p < 0.05$ ). (b) The spatial extent of the three auditory cortex probability maps for the same 4 axial slices as (a), which include Heschl's Gyrus (Penhune et al., 1996), containing both primary (Morosan et al., 2001) and secondary auditory cortex, as well as the regions immediately posterior and superior, corresponding to planum temporale (Westbury et al., 1999).

**Figure 4:** (a) Group random effects SPM t-statistic images showing all suprathreshold voxels where BOLD activity showed a 1<sup>st</sup> order (linear) polynomial covariation with IAC level, for four axial slices superimposed over an individual T1 image. Slice positions ( $\pm$  white) are given in MNI z coordinates. All images show small-volume corrected (AC-ROI) thresholds ( $t > 5.22$ ,  $p < 0.05$ ). (b) The same four axial slices showing three cytoarchitectural subdivisions of primary auditory cortex (Te1.1, Te1.0, and TE1.2) (Morosan et al, 2001).

**Figure 5:** Mean raw (adjusted) BOLD signal averaged across all suprathreshold voxels that showed a significant linear covariation with IAC level in Figure 4 (a).

Table 1: Mean percentage (standard error) of key-press responses that proceeded volume acquisitions within the required 2-s time window. Results are given for each level of IAC ( $\rho$ ) and for the silent baseline.

Noise						Silence
$\rho$						
0.00	0.33	0.60	0.80	0.93	1.00	
87.2	87.1	84.7	86.8	86.3	84.7	84.2
(5.49)	(5.26)	(5.81)	(5.31)	(5.71)	(6.55)	(5.59)

Table 2:  $0^{\text{th}}$ -order polynomial effect: Anatomical locations, coordinates, and probabilities that activation maxima in Figure 3a reside within cytoarchitecturally defined auditory cortical areas. All peak t values are significant ( $p < 0.05$ , corrected). All probability values are expressed as a percentage of the maximum probability value within each map.

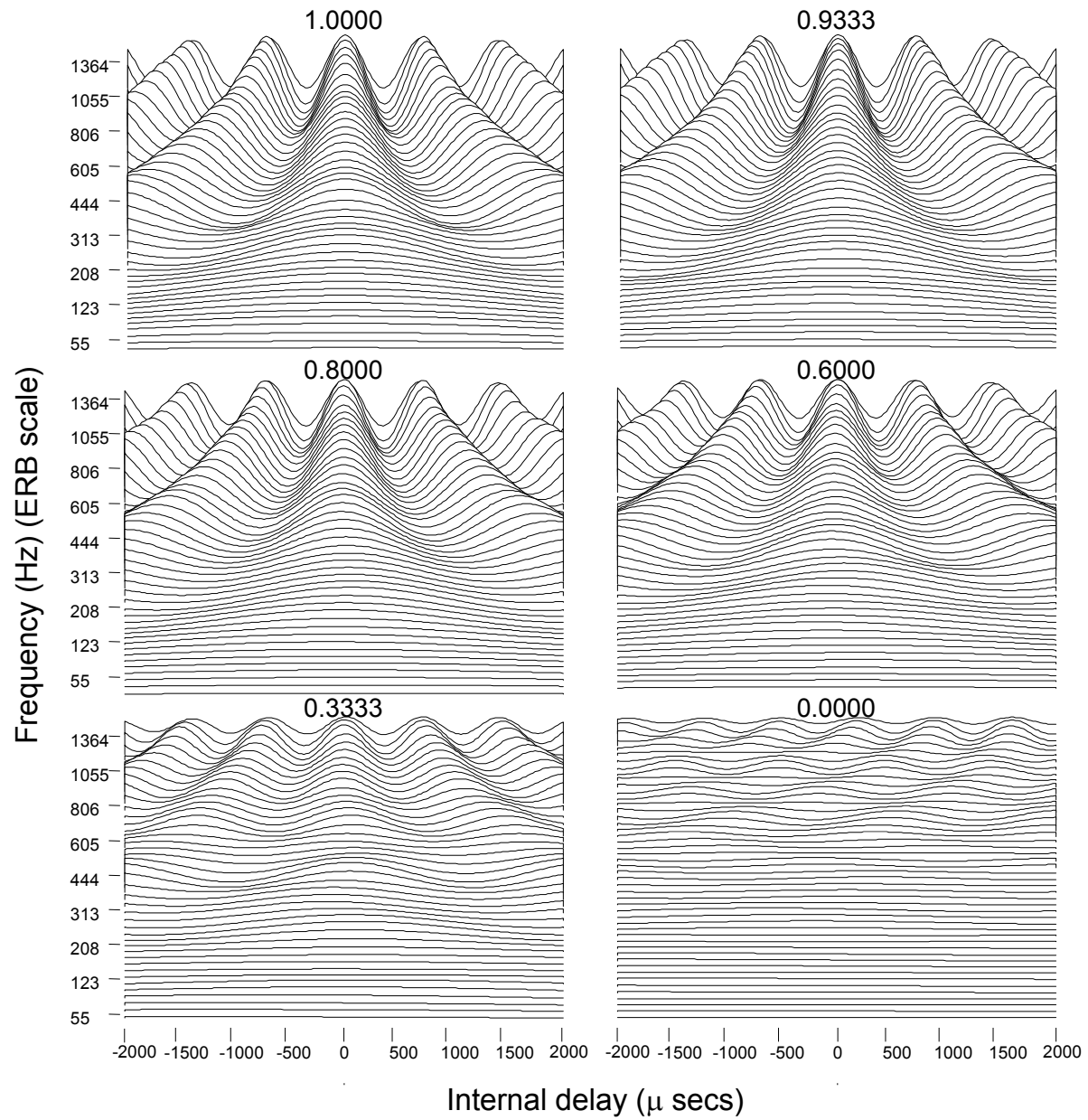
Talairach Label (Brodmann Area)	MNI xyz	Talairach xyz	Probability					Peak t values
			Morosan PAC			Penhune	Westbury	
			Te1.0	Te1.1	Te1.2	HG	PT	
L STG (41)	-48 -16 +4	-47 -16 +5	12	0	0	70	0	11.03
L STG (42)	-62 -26 +8	-61 -25 +9	0	0	0	0	64	9.81
R HG (22)	+42 -24 +10	-42 -23 +10	0	13	0	55	8	8.49
R STG (22)	+51 -6 +0	-51 -6 +0	19	0	33	41	0	9.40

L: left; R: right; STG: superior temporal gyrus; HG: Heschl's gyrus; PT: planum temporale.

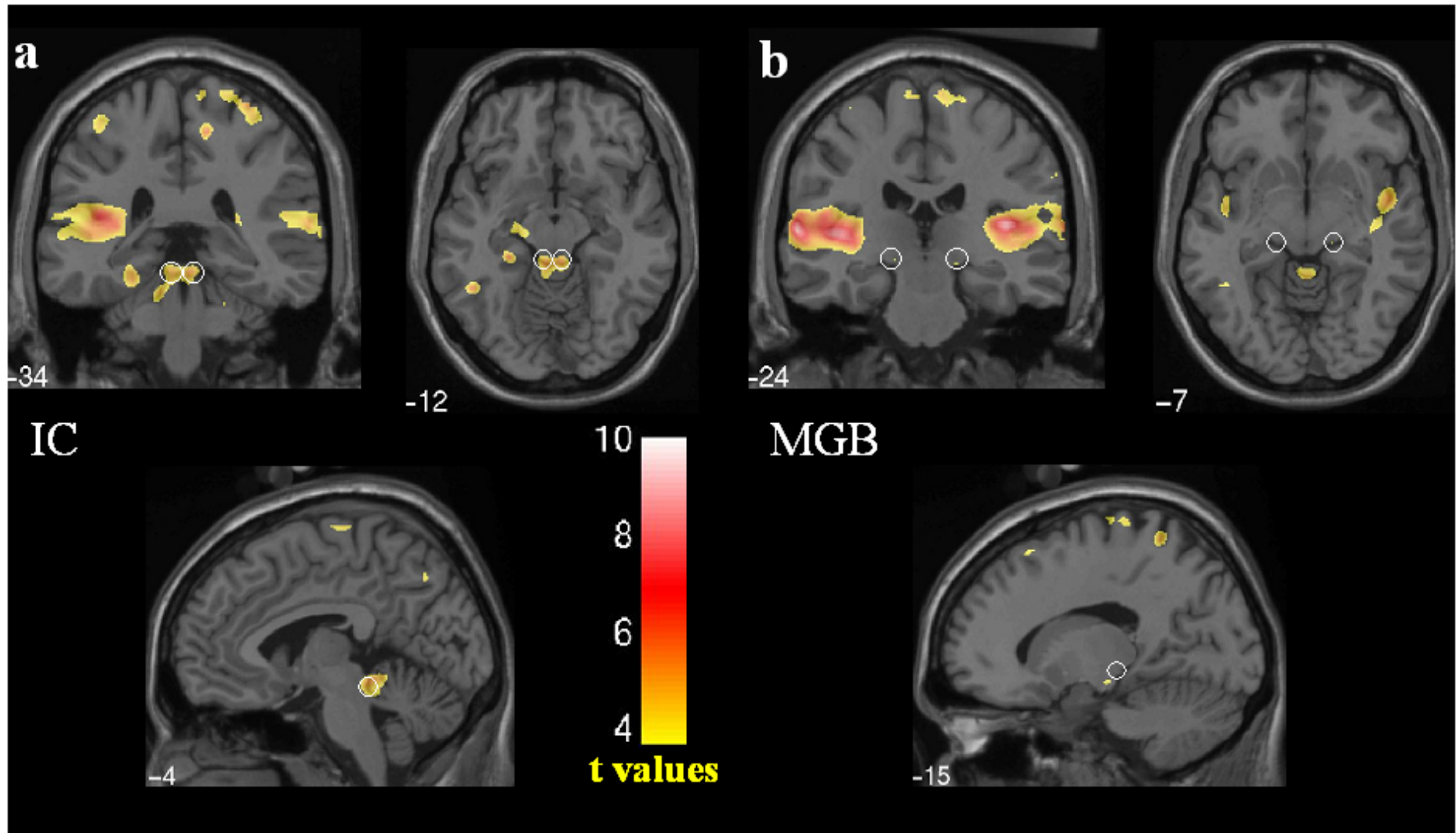
Table 3. *1<sup>st</sup>-order polynomial effect*: Anatomical locations, coordinates, and probabilities that activation maxima in Figure 4a reside within specified auditory cortical areas. All t values are significant ( $p < 0.05$ , corrected). All probability values are expressed as a percentage of the maximum probability value within each map.

Talairach Label (Brodmann Area)	MNI xyz	Talairach Xyz	Probability					t
			Morosan			Penhune	Westbury	
			Te1.0	Te1.1	Te1.2	HG	PT	
L STG (22)	-56 -8 +2	-55 -8 +2	0	0	50	23	5	6.10
R STG (22)	+56 -2 +4	+55 -2 +4	26	0	66	29	3	6.82

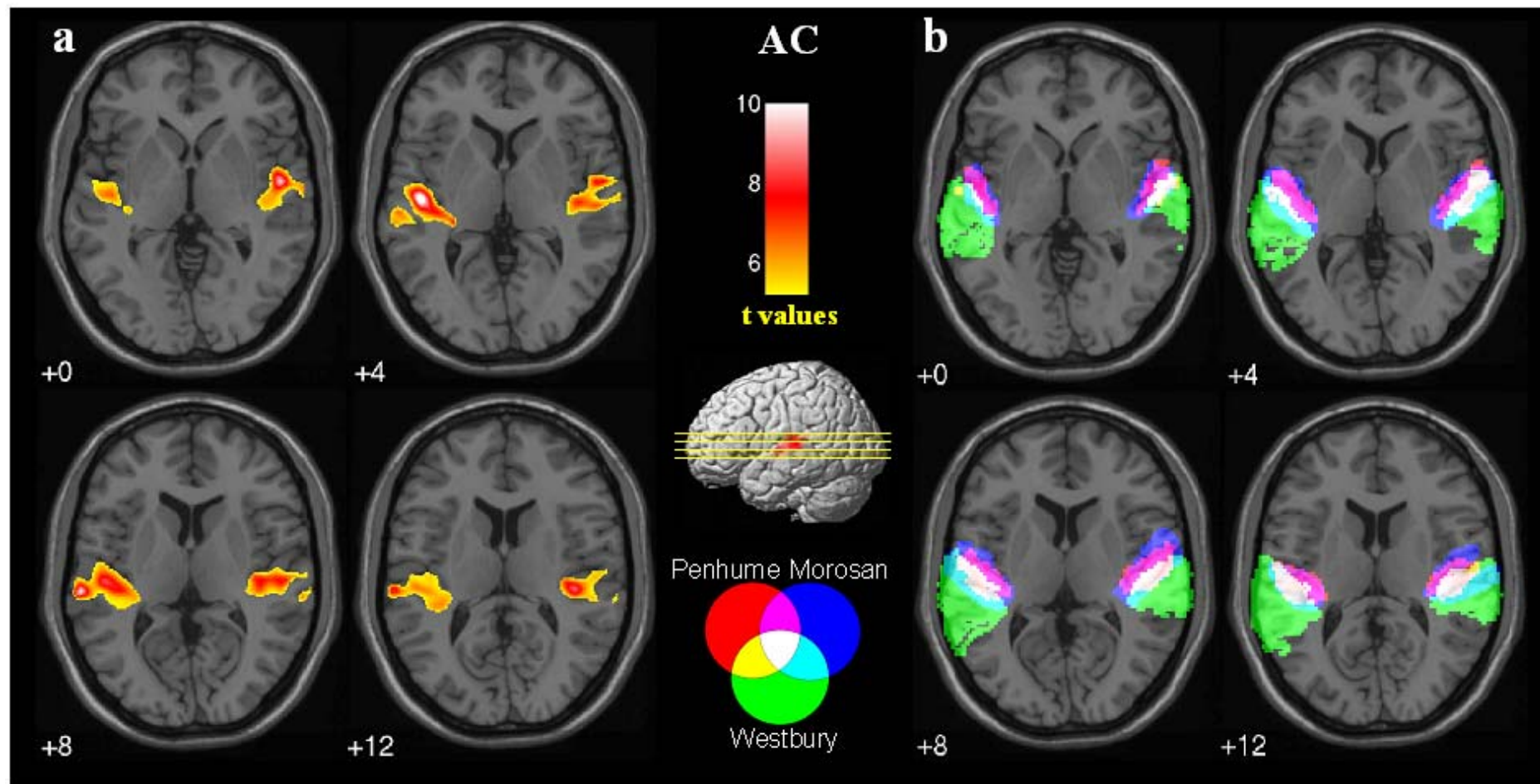
L: left; R: right; STG: superior temporal gyrus; HG: Heschl's gyrus; PT: planum temporale.



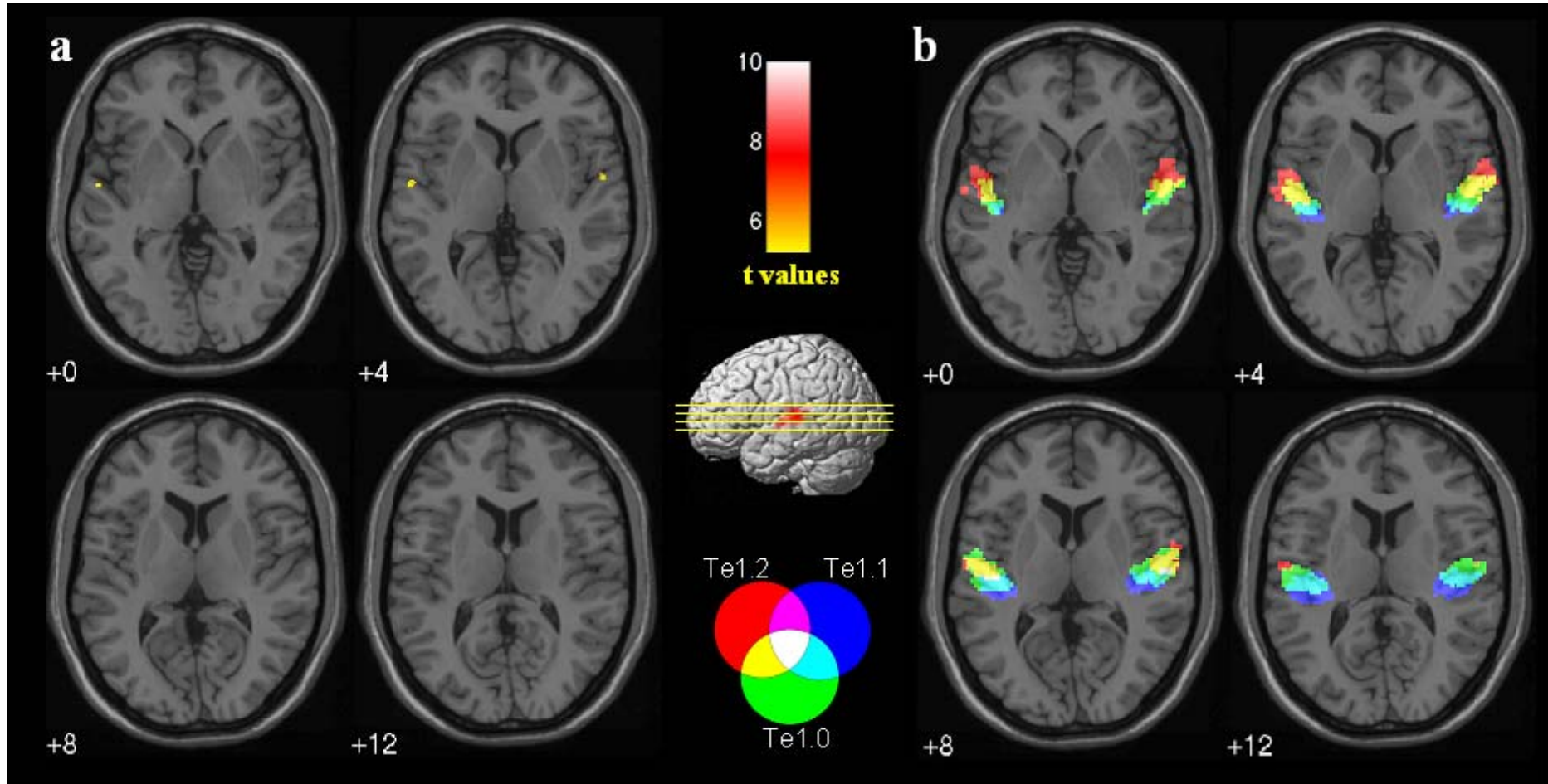
Budd et al.: Figure 1



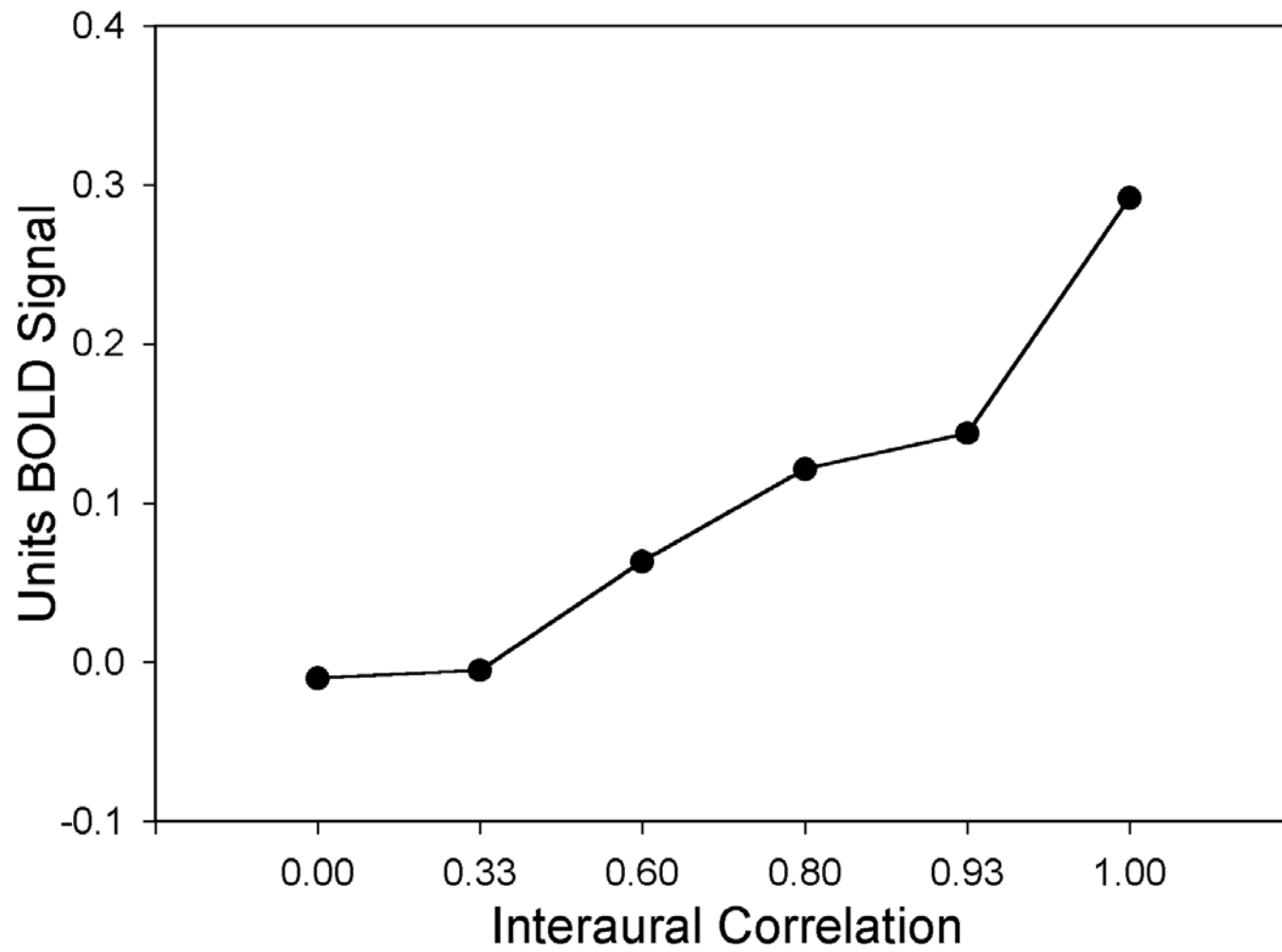
Budd et al.: Figure 2



Budd et al.: Figure 3



Budd et al.: Figure 4



Budd et al.: Figure 5